AFRL-AFOSR-VA-TR-2022-0696

MEMS-Based Platform for Quantum Information Processing with Spins in Diamond

Hailin Wang
University of Oregon, Eugene OR
5219 UNIVERSITY OF OREGON
EUGENE, OR, 97403-3120
US

09/29/2022
Final Technical Report

Air Force Research Laboratory
Air Force Office of Scientific Research
Arlington, Virginia 22203
Air Force Materiel Command

REPORT DOCUMENTATION PAGE

PLEASE DO NOT RETURN YOUR FORM TO THE ABOVE ORGANIZATION.

1. REPORT DATE	2. REPORT TYPE	3. DATES COVERED	
20220929	Final	START DATE 20160930	END DATE 20200929

4. TITLE AND SUBTITLE
MEMS-Based Platform for Quantum Information Processing with Spins in Diamond

5a. CONTRACT NUMBER	5b. GRANT NUMBER	5c. PROGRAM ELEMENT NUMBER
	FA9550-16-1-0424	61102F
5d. PROJECT NUMBER	**5e. TASK NUMBER**	**5f. WORK UNIT NUMBER**

6. AUTHOR(S)
Hailin Wang

7. PERFORMING ORGANIZATION NAME(S) AND ADDRESS(ES)
University of Oregon, Eugene OR
5219 UNIVERSITY OF OREGON
EUGENE, OR 97403-3120
US

8. PERFORMING ORGANIZATION REPORT NUMBER

9. SPONSORING/MONITORING AGENCY NAME(S) AND ADDRESS(ES)	10. SPONSOR/MONITOR'S ACRONYM(S)	11. SPONSOR/MONITOR'S REPORT NUMBER(S)
Air Force Office of Scientific Research 875 N. Randolph St. Room 3112 Arlington, VA 22203	AFRL/AFOSR RTB1	AFRL-AFOSR-VA-TR-2022-0696

12. DISTRIBUTION/AVAILABILITY STATEMENT
A Distribution Unlimited: PB Public Release

13. SUPPLEMENTARY NOTES

14. ABSTRACT
This program exploits diamond nanomechanical structures to develop a platform for quantum computing. In this platform, defect centers such as nitrogen vacancy (NV) or silicon vacancy (SiV) centers couple to compression mechanical vibrations in a Lamb wave resonator (LWR). The resulting spin-mechanical interactions can be used to mediate coherent interactions between electron spins. The platform can be viewed as a solid-state analog of trapped ions. Research efforts carried out in this program have focused on tasks that are crucial for the experimental realization of a solid-state analog of trapped ions. Diamond LWRs implanted with either NV or SiV centers have been successfully fabricated. Soft-plasma-etching based surface treatment, which overcomes complications due to surface charge fluctuations in diamond, has been developed. Phononic networks, which consist of diamond LWRs and alternating phononic crystal waveguides and features an architecture of closed mechanical subsystems, have been designed and theoretically analyzed. This architecture enables nearest neighbor mechanically mediated coupling between spins and circumvents the scaling problems inherent in conventional phononic networks. Strong coherent spin-mechanical interactions via orbital strain coupling have been demonstrated. In addition, robust and nonreciprocal transport of phonons in phononic waveguides have also been explored.

15. SUBJECT TERMS

16. SECURITY CLASSIFICATION OF:			17. LIMITATION OF ABSTRACT	18. NUMBER OF PAGES
a. REPORT U	b. ABSTRACT U	c. THIS PAGE U	UU	19

19a. NAME OF RESPONSIBLE PERSON	19b. PHONE NUMBER *(Include area code)*
GRACE METCALFE	(703) 696-9740

REPORT DOCUMENTATION PAGE

Form Approved
OMB No. 0704-0188

1. REPORT DATE *(DD-MM-YYYY)*	2. REPORT TYPE	3. DATES COVERED *(From - To)*
25-01-2021	Final technical	Oct. 2016 - Sept. 2020

4. TITLE AND SUBTITLE
MEMS-Based Platform for Quantum Information Processing with Spins in Diamond

5a. CONTRACT NUMBER
FA9550-16-1-0424

5b. GRANT NUMBER

5c. PROGRAM ELEMENT NUMBER

6. AUTHOR(S)
Hailin Wang, University of Oregon
Gaurav Bahl, Univ. of Illinois,

5d. PROJECT NUMBER

5e. TASK NUMBER

5f. WORK UNIT NUMBER

7. PERFORMING ORGANIZATION NAME(S) AND ADDRESS(ES)
Department of Physics, University of Oregon, Eugene, OR 97403
Mechanical Science and Engineering, Univ. of Illinois at Urbana-Champaign, IL

8. PERFORMING ORGANIZATION REPORT NUMBER

9. SPONSORING/MONITORING AGENCY NAME(S) AND ADDRESS(ES)
AFOSR
801 N Randolph St., Rm. 732, Arlington VA 22203

10. SPONSOR/MONITOR'S ACRONYM(S)

11. SPONSOR/MONITOR'S REPORT NUMBER(S)

12. DISTRIBUTION/AVAILABILITY STATEMENT

13. SUPPLEMENTARY NOTES

14. ABSTRACT

This program exploits diamond nanomechanical structures to develop a platform for quantum computing. In this platform, defect centers such as nitrogen vacancy (NV) or silicon vacancy (SiV) centers couple to compression mechanical vibrations in a Lamb wave resonator (LWR). Research efforts carried out in this program have focused on fabrication and characterization of diamond LWRs implanted with NVs and SiVs, design and theoretical analysis of scalable phononic networks, demonstration of strong coherent spin-mechanical interactions in diamond, and robust and nonreciprocal transport of phonons in phononic waveguides.

15. SUBJECT TERMS

nitrogen vacancy centers, silicon vacancy centers, spin-mechanics, spin coherence, Lamb wave resonator, surface acoustic wave, diamond nano-fabrication, phononic band gaps, phononic waveguides, quantum computing, quantum gates, quantum information processing

16. SECURITY CLASSIFICATION OF:			17. LIMITATION OF ABSTRACT	18. NUMBER OF PAGES	19a. NAME OF RESPONSIBLE PERSON
a. REPORT	b. ABSTRACT	c. THIS PAGE			19b. TELEPHONE NUMBER *(Include area code)*
U	U	U	UU	18	

Final Technical Report

MEMS-Based Platform for Quantum Information Processing with Spins in Diamond

Oct. 1, 2016 – Sept. 30, 2020

Principal Investigator: Hailin Wang
Department of Physics
University of Oregon
Eugene, OR 97403
Phone: 541-346-4758; hailin@uoregon.edu

Co-PI: Gaurav Bahl
Mechanical Science and Engineering
Univ. of Illinois at Urbana-Champaign
Phone: 217-300-2194; bahl@illinois.edu

Grant Number: FA9550-16-1-0424

AFOSR program manager: Dr. Grace Metcalfe

Abstract

This program exploits diamond nanomechanical structures to develop a platform for quantum computing. In this platform, defect centers such as nitrogen vacancy (NV) or silicon vacancy (SiV) centers couple to compression mechanical vibrations in a Lamb wave resonator (LWR). The resulting spin-mechanical interactions can be used to mediate coherent interactions between electron spins. The platform can be viewed as a solid-state analog of trapped ions.

Research efforts carried out in this program have focused on tasks that are crucial for the experimental realization of a solid-state analog of trapped ions. Diamond LWRs implanted with either NV or SiV centers have been successfully fabricated. Soft-plasma-etching based surface treatment, which overcomes complications due to surface charge fluctuations in diamond, has been developed. Phononic networks, which consist of diamond LWRs and alternating phononic crystal waveguides and features an architecture of closed mechanical subsystems, have been designed and theoretically analyzed. This architecture enables nearest neighbor mechanically mediated coupling between spins and circumvents the scaling problems inherent in conventional phononic networks. Strong coherent spin-mechanical interactions via orbital strain coupling have been demonstrated. In addition, robust and nonreciprocal transport of phonons in phononic waveguides have also been explored.

TABLE OF CONTENTS

Page

Cover

1. STATEMENT OF PROBLEMS STUDIED

This program aims to develop a platform for quantum computing by using electron spins in diamond nanomechanical structures. In this platform, defect centers such as nitrogen vacancy (NV) or silicon vacancy (SiV) centers couple to compression mechanical vibrations in a Lamb wave resonator (LWR). The spin-mechanical interactions can be used for the generation of entanglement between electron spins and for the implementation of two-qubit quantum gates. The platform resembles the well-known trapped-ion system, which is among the most successful for quantum information processing.

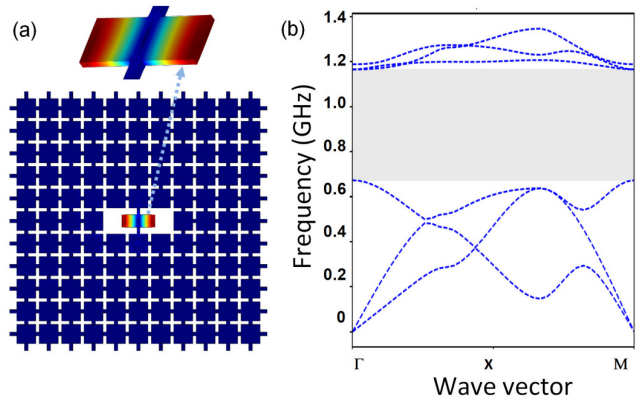

Fig. 1. a) A diamond Lamb wave resonator (4.5 μm by 9.5 μm) embedded in a square phononic crystal lattice with a period of 8 μm, along with the calculated displacement pattern for the fundamental compression mode at 0.95 GHz. (b) Phononic band structure of the symmetric compression modes in the square lattice. The shaded area highlights the phononic band gap.

The spin-nanomechanical system pursued in this program has two key components: i) defect centers such as NV or SiV centers that feature robust spin coherence as well as strong spin-mechanical coupling (via either ground- or excited-state strain coupling); ii) LWRs that feature high-Q GHz compression modes. With the LWRs embedded in a phononic band gap structure as shown in Fig. 1, the symmetric compression modes in the LWR can be effectively decoupled from the surrounding environment, which can lead to Q-factors limited only by the intrinsic material loss of diamond.

Research efforts carried out in this program have focused on four tasks that are crucial for the development of a solid-state analog of trapped ions: i) fabrication and characterization of diamond LWRs implanted with NV or SiV centers; ii) design and theoretical analysis of scalable phononic networks consisting of diamond LWRs and phononic waveguides; iii) demonstration of strong coherent spin-mechanical interactions in diamond; iv) robust and nonreciprocal transport of phonons in phononic waveguides. Important results obtained in this program are summarized in Section 2 (the references cited are listed in Section 3).

2. SUMMARY OF IMPORTANT RESULTS

i) Fabrication and characterization of diamond LWRs embedded in a phononic crystal

A thin elastic plate with free boundaries serves naturally as a mechanical resonator. The eigen modes of the thin plate are characterized by Lamb waves or Lamb modes. The mechanical Q-factor is only limited by the clamping loss and the intrinsic acoustic attenuation of the elastic material. By embedding the resonator in a phononic crystal and with the mechanical frequencies in the phononic bandgap, we can essentially eliminate the clamping loss.

a) Fabrication [1]

We have successfully fabricated diamond LWRs embedded in a square phononic crystal lattice. The fabrication started with an electronic grade single-crystal diamond film with a thickness about 30 μm. The slicing and polishing of a chemical-vapor-deposition grown bulk diamond sample (Element Six, Inc.) into the thin film were carried out by Applied Diamond, Inc. Figure 2a shows the flow chart of the fabrication process.

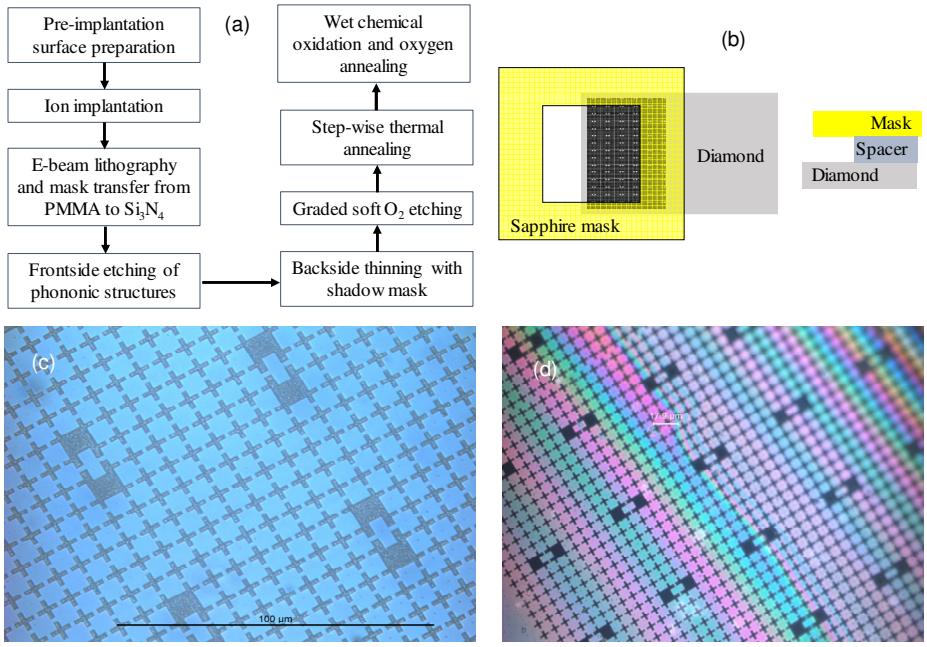

Fig. 2. (a) Flowchart for the fabrication of diamond Lamb wave resonators embedded in a phononic crystal lattice. (b) Schematic of backside thinning with a shadow mask. A spacer with a thickness of 150 μm is used to avoid trenching. (c) Optical image of a 2D phononic structure with a thickness about 30 μm, for which the structure is not yet released. (b) Optical image of a 2D phononic structure (with a thickness < 1 μm), which is completely released. The period of the square phononic crystal lattice in the two images is 8 μm.

The key steps include the implantation/creation of NV centers about 100 nm below the diamond surface, the electron beam lithography, mask transfer from Polymethyl methacrylate (PMMA) to Si_3N_4, reactive ion etching (RIE) of the phononic nanostructure on the front (i.e., the implanted) side, thinning of the diamond membrane from about 30 µm to less than 1 µm from the backside. The implantation was carried out at a commercial foundry (Innovion, Inc). The RIE was carried out in a PlasmaPro NGP80 ICP65 etcher from Oxford Instrument. The details of the fabrication process are discussed in [1].

An important feature of our fabrication approach is the use of a sapphire shadow mask during the backside thinning of the diamond film (see Fig. 2b). We positioned the sapphire mask, along with a 150 µm thick spacer, at one edge of the diamond film, with an etching area approximately 1.5 mm by 0.75 mm. In this way, the suspended phononic structure is attached or anchored to the bulk diamond film in three sides. The shadow mask not only defines the area of the diamond film that will be thinned down, but also avoids the trenching that occurs when the mask is in direct contact with the sample.

Figure 2c shows an optical image of a 2D phononic structure (with the design shown in Fig. 1a) etched in a 30 µm thick diamond film. Figure 2d shows an optical image of a completely released 2D phononic structure with a thickness < 1 µm. The color fringes in Fig. 2d are due to slight variations in the thickness of the released structure. These variations, which occurred during the slicing and polishing of the bulk diamond film, can be minimized or corrected. The optical interference fringes can also be used for the measurement of the membrane thickness. Figure 3a shows a scanning electron microscope (SEM) image of a released LWR. A confocal optical image of a released LWR showing NV centers in the resonator is displayed in Fig. 3b.

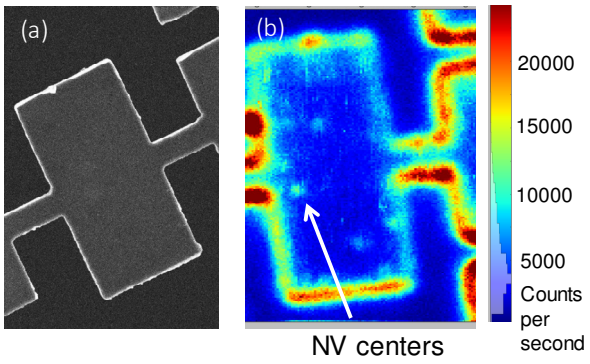

Fig. 3. (a) A SEM image of a released Lamb wave resonator, with a dimension of 9.5 µm by 4.5 µm. (b) Confocal optical image showing NV centers in a released Lamb wave resonator.

b) Characterization and diamond surface treatment [1]

NV centers are highly sensitive to surface charge fluctuations, leading to excessive spectral diffusion and poor optical coherence in thin membranes. Previous studies in this area have shown an optical linewidth exceeding 1 GHz for NV centers in membranes with a thickness about 1 μm. Similar results have also been observed in our samples, as shown in the photoluminescence excitation (PLE) spectrum in Fig. 4a. The large NV linewidth is due to the charge fluctuations in the surface layers damaged by the RIE on the backside. For comparison, NV linewidth obtained before the backside thinning, but after the fabrication of the phononic nanostructure on the front side is close to 100 MHz, as shown in Fig. 4b.

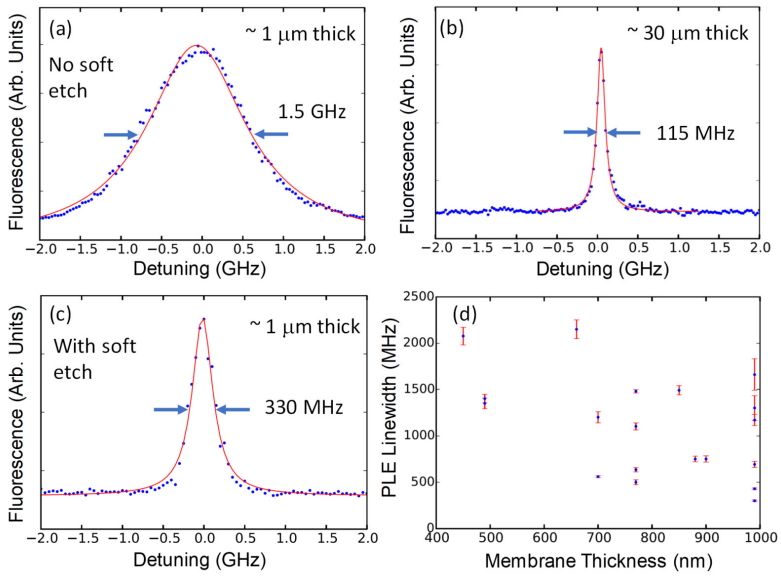

Fig. 4. (a) PLE spectrum of a NV in a released LWR with a thickness near 1 μm and without soft O_2 etch. (b) PLE spectrum of a NV obtained before the backside thinning, but after the frontside RIE. (c) PLE spectrum of a NV in a released LWR with a thickness near 1 μm and with soft O_2 etch. Red lines in these spectra are least square fits to a Lorentzian. (d) A scatter plot of PLE linewidths for NVs in released LWRs with varying thicknesses, obtained under conditions similar to those in (c). All data were taken at T~ 8 K.

We have developed a graded soft O_2 plasma etching technique, with the slowest etching rate significantly below 1 nm/min. The goal of this technique is to remove damaged surface layers without causing additional damages. The graded soft etching significantly improves the NV optical coherence. As shown in Fig. 4c, the graded soft etching reduces the optical linewidth of a NV center in a 1 μm thick membrane from 1.5 GHz (see Fig. 4a) to as small as 330 MHz. Nevertheless, for membranes with a thickness less than 500 nm, the NV optical linewidth still broadens to beyond 1 GHz, even after graded soft etching and extensive surface treatment, as shown in Fig. 4d. Note that spectral broadening due to surface charge fluctuations can be avoided in SiV centers in similarly prepared membranes with a thickness as small as 100 nm, as discussed in the next sub-section.

c) Optical coherence of SiV centers in thin diamond membranes [2]

Because of their symmetry properties, optical transitions in negatively charged SiV centers can be robust against surface charge fluctuations. In the absence of an external magnetic field, both the ground and excited states of a SiV center are doublets due to spin-orbit interactions, as shown schematically in Fig. 5a. The spin-orbit splitting for the ground and excited states is λ_{so}^{g} =47 GHz and λ_{so}^{u} =260 GHz, respectively. All transitions between the ground and excited states are dipole-allowed. Figure 5b shows as an example a PLE spectrum obtained in a 30 μm thick film and at a temperature of 12 K. Multiple SiV centers are observed within the effective detection area of our confocal setup. Figure 5c shows a PLE spectrum in the 30 μm thick film with a spectral range over 175 GHz. For this spectrum, we stitched together five PLE spectra of individual scans with a scan range of 40 GHz. From the extended PLE spectrum, we can identify the overall ground-state splitting of the SiV centers, in general agreement with the theoretical expectation.

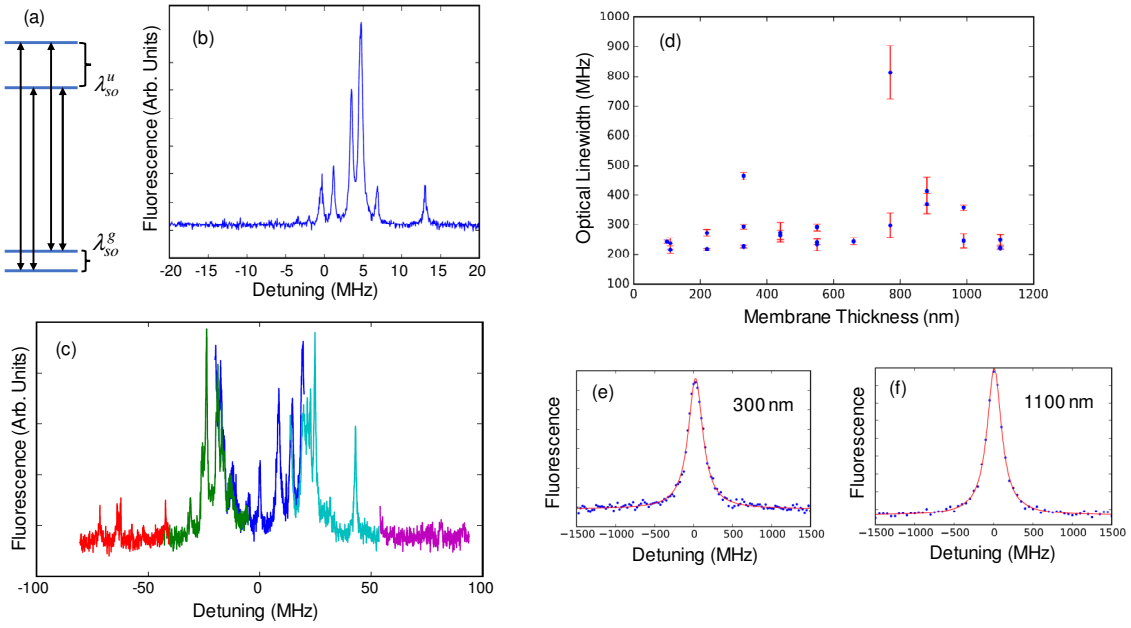

Fig. 5. (a) Schematic of the optical transitions in a SiV center (with no strain). (b) A PLE spectrum obtained near the SiV optical transition wavelengths. (c) An extended scan of a PLE spectrum, combining together five individual scans. (d) A scatter plot of the optical linewidths for SiV centers in diamond membranes with varying thicknesses. (e) PLE spectrum of a SiV center in a membrane with a thickness of 330 nm. (f) PLE spectrum of a SiV center in a membrane with a thickness of 1100 nm. Red lines in (e) and (f) are least square fits to a Lorentzian, showing a linewidth of 226 MHz for (b) and 222 MHz for (c). All data were obtained at 12 K.

Figure 5d plots the optical linewidths obtained for SiV centers in membranes with a thickness ranging from 100 nm to 1100 nm. For the 22 SiV centers studied, 20 SiV centers exhibit linewidths between 200 to 400 MHz, while 17 SiV centers have linewidths between 200 and 300 MHz. Furthermore, there is no discernable dependence of the SiV optical linewidth on the membrane thickness. Figures 5e and 5f show SiV optical resonances obtained in membranes with estimated thickness of 330 nm and 1100 nm, respectively. A least square fit to a Lorentzian gives an optical linewidth of 226 MHz and 222 MHz for SiV centers in 330 and 1100 nm thick membranes, respectively.

ii) Scalable phononic networks with closed mechanical subsystems [3,4]

We have developed an architecture for phononic quantum networks of spins in diamond, which exploits phononic bandgap engineering to form closed mechanical subsystems. This architecture overcomes the inherent obstacles in scaling phononic quantum networks and avoids the technical difficulty of employing chiral spin-phonon interactions, providing a promising route for developing quantum computers using robust solid-state spin qubits. A key element of the architecture is the use of alternating phononic crystal waveguides that feature specially designed bandgaps. In this network, phononic waveguides enable the coupling between adjacent resonators. The specially designed phononic bandgaps in the alternating waveguides, however, prevent the propagation of the relevant mechanical vibration to nearby waveguides, as shown in the numerical simulation displayed in Fig. 6a.

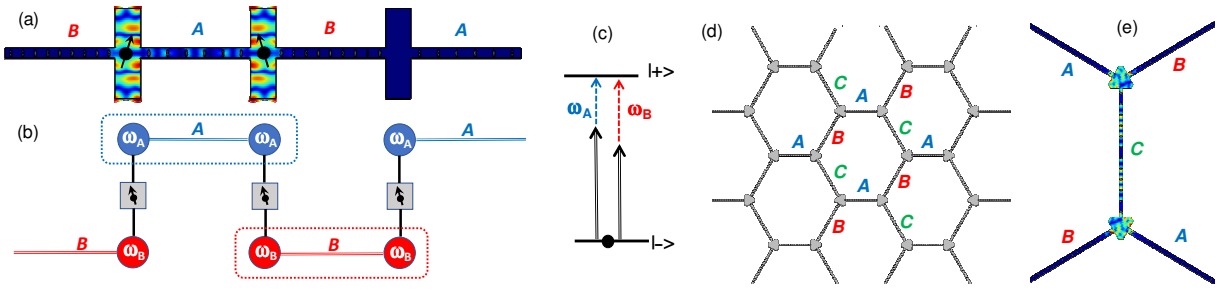

Fig. 6. (a) Displacement pattern of a normal mode in a 1D phononic network with alternating phononic crystal waveguides. (b) Schematic of the network architecture. The dashed-line boxes illustrate closed mechanical subsystems. (c) Coupling a spin qubit to two resonator modes via sideband transitions. (d) A honeycomb lattice, for which each resonator couples to three distinct phononic crystal waveguides *A*, *B*, and *C*. (e) The displacement pattern of a mechanical normal mode, which propagates in waveguide *C*, but is forbidden in *A* and *B*, leading to a closed subsystem containing waveguide *C* and the two directly connected resonators.

For rectangular LWRs in a 1D network (see Fig. 6a), we design/select two resonator modes (the ω_A and ω_B modes in Fig. 6b) such that each mode couples only to one of the two adjacent waveguides (this occurs when the resonator mode is in the bandgap of the other waveguide). As a result, any two adjacent mechanical resonators and the waveguide between them can form a closed mechanical subsystem, as illustrated in Fig. 6b and demonstrated by the numerical simulation of the mechanical displacement pattern in Fig. 6a. This closed mechanical subsystem enables the nearest neighbor coupling between spins in adjacent resonators and circumvents the scaling problem in conventional mechanical networks. Another essential feature of our architecture is that for a given resonator, a spin qubit can couple to both selected resonator modes, which can take place, for example, via sideband transitions, as illustrated in Fig. 6c. In this way, the closed mechanical subsystems are networked together via the multi-mode spin-mechanical coupling process, as illustrated in Fig. 6b.

We have also extended this architecture to a 2D network, which can in principle enable topological quantum error corrections. Figure 6d shows a honeycomb-like phononic network, in which each triangular-shaped mechanical resonator is connected to three distinct phononic crystal waveguides with specially designed phononic bandgaps. Similar to the 1D network, we design/select three resonator modes such that each mode couples only to one of the three waveguides. In this case, any two adjacent mechanical resonators and the waveguide between them can form a closed mechanical subsystem, as shown by the numerical simulation of the mechanical displacement pattern shown in Fig. 6e. The phononic network can also be embedded in a phononic crystal lattice, which isolates and protects the relevant mechanical modes of the phononic network.

iii) Dark-state mediated spin-mechanical interactions and state transfers

a) Strong spin-mechanical interactions via a dark state [5, 6]

Robust spin coherence in a NV center necessarily means extremely weak coupling between the spin and the acoustic vibrations, since otherwise the coupling will lead to rapid decay of the spin coherence. Nevertheless, the orbital degrees of freedom associated with the excited states of a NV center can feature much stronger strain coupling to acoustic vibrations. The deformation potential, which characterizes the strength of the excited-state strain coupling, scales with the relevant energy gap and is five orders of magnitude greater than the

corresponding parameter for the ground-state strain coupling. The excited states, however, are not suitable for use as qubits because an electron in these states can quickly decay to the ground spin states through optical spontaneous emission.

To overcome this dilemma, we have coupled an acoustic wave to a NV electron spin qubit through an optically prepared dark state in a Λ-type three-level system. A key ingredient of this process is to use the strain coupling of an excited state to mediate the interaction between the acoustic wave and the NV spin states, but without populating the excited state. This scheme exploits the optically prepared dark state, which traps the electron in the ground spin states through quantum interference or through adiabatic evolution of the spin states. Our experiments demonstrate that we can take advantage of the strong excited-state electron-phonon interaction to mediate and control the coupling between spin and mechanical degrees of freedom, while avoiding decoherence associated with the excited state.

As illustrated in Fig. 7a, the experimental demonstration is based on the use of surface acoustic waves (SAWs), which propagate along and extend approximately one acoustic wavelength below the diamond surface. For the samples used in our experiments, a 400 nm thick ZnO layer, which is piezoelectric, is sputtered onto the diamond surface. The SAW is generated by an interdigital transducer (IDT) patterned on the ZnO layer (see Fig. 6b). The center frequency of the IDT is near 900 MHz.

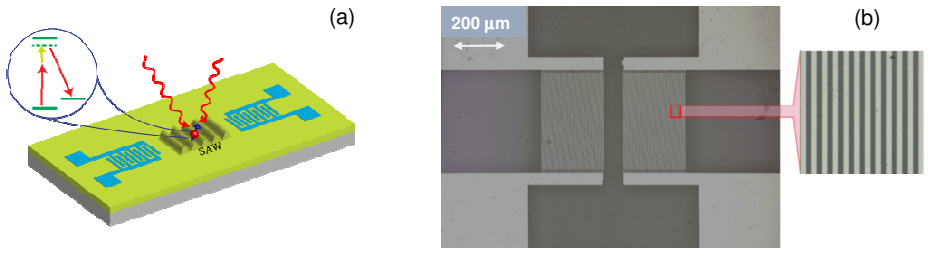

Fig. 7. (a) Schematic of a NV center driven by two optical fields and a SAW field generated by an IDT. (b) Optical image of a pair of IDTs fabricated on the diamond surface.

The Λ-type three-level system we have used consists of the E_y state as the upper state, the m_s=0 state as one of the lower states, and either the m_s=+1 or -1 state as the other lower state (see Fig. 8a). Figure 8b shows the fluorescence from the E_y state as a function of detuning, $\omega_0+\omega_m-\omega_\pm$, for which the NV was initially prepared in the m_s=0 state. Two pronounced dips are observed in Fig. 8b when the Raman resonant condition is satisfied, i.e. when $\omega_0+\omega_m-\omega_\pm$ equals

the frequency separation between the m_s=0 and the m_s=±1 states. Two sets of Λ-type systems are involved in this case. One contains the m_s=+1 state and the other the m_s=-1 state. The two dips in Fig. 8b correspond to the quenching of the NV fluorescence when the NV is pumped into the respective dark state. These dips are a direct manifestation of the phonon-assisted coherent population trapping (CPT) process, demonstrating the coherent interaction between the SAW and the relevant electron spin coherence.

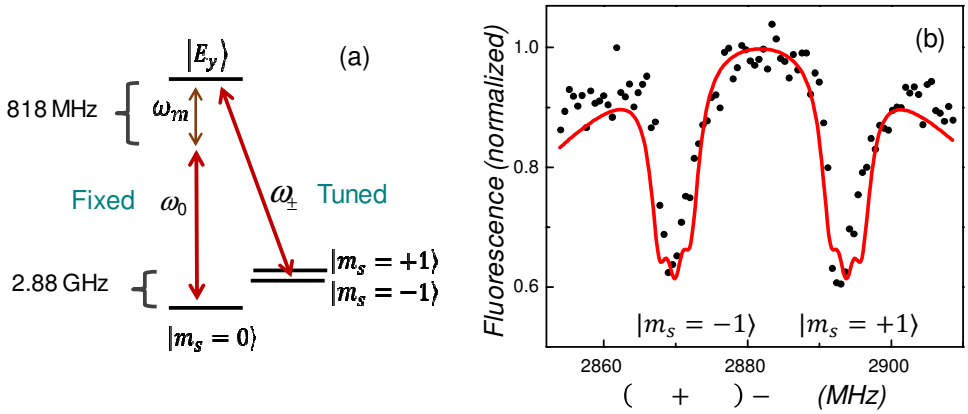

Fig. 8. (a) Energy level diagram used for phonon-assisted CPT. Solid red arrows are the optical fields. Dashed brown arrow is the acoustic field. (b) Fluorescence from state E_y as a function of $\omega_0+\omega_m-\omega_\pm$. The two dips correspond to CPT associated with Λ-type systems formed with either the m_s=+1 or the m_s= −1 state.

For the phonon-assisted CPT discussed above, the residual excitation and subsequent decay of the upper state in the Λ-type system introduces an optically induced decoherence to the spin-phonon system. With a conventional Λ-type system, the upper state can be eliminated adiabatically from the dynamics of the two lower states, if the two optical driving fields are sufficiently detuned from the respective dipole optical transitions. In this adiabatic limit, the three-level system becomes equivalent to an optically driven spin transition between the two lower states. In analogy, for a Λ-type three-level system coupling to an acoustic as well as two optical fields and with a sufficiently large detuning for both the optical and the phonon-assisted optical transitions, the three-level system becomes equivalent to optically driven spin transitions between the phonon ladders of the two lower states, or the sideband spin transitions. We have demonstrated the optically driven sideband spin transitions in the spectral as well as the time domain. The time domain experiment provides additional information on the residual excitation of the excited state in the Λ-type three-level systems [5].

b) Transfer of phase information between optical and microwave fields via a dark state [7]

The dark state in a NV center can also be used for the quantum state transfer between optical and microwave fields. Specifically, we demonstrate that a single NV center in diamond can enable the transfer of phase information between microwave and optical fields. We map the relative phase of two microwave fields to a superposition spin state in a NV center and then read out the phase with two optical fields. A closely related process is used for the transfer of phase information from optical to microwave fields. The dark state, which is decoupled from either optical or microwave fields, plays a central role in the phase transfer process. Similar coherent coupling in a NV ensemble can enable the full quantum-state transfer between microwave and optical fields.

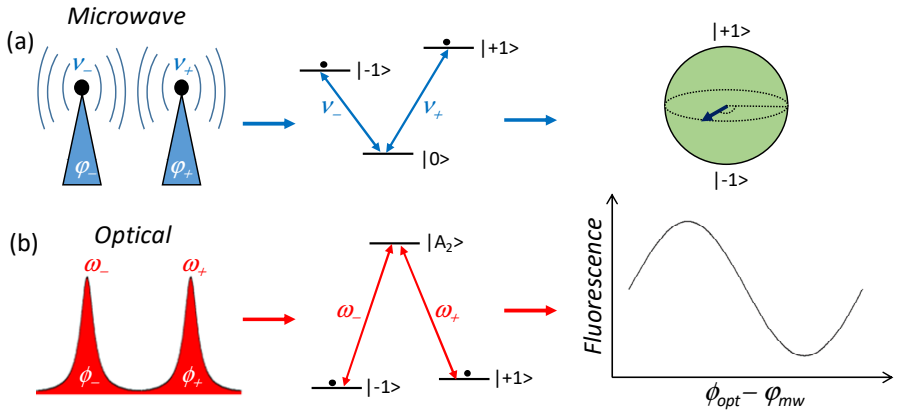

Fig. 9. a) Two microwave fields, with relative phase, $\varphi_{mw} = \varphi_+ - \varphi_-$, couple resonantly to the m_s=0 to $m_s = \pm 1$ transitions and generate a coherent superposition of the $m_s = \pm 1$ states, effectively mapping φ_{mw} to the phase of the spin coherence. (b) Two optical fields, with relative phase, $\phi_{opt} = \phi_+ - \phi_-$, couple resonantly to the $m_s = \pm 1$ to A_2 transitions. The fluorescence from the A_2 state features sinusoidal oscillations as a function of $\phi_{opt} - \varphi_{mw}$, effectively reading out the relative microwave phase and transferring the phase information from the microwave to the optical fields.

Our scheme for coherent coupling between optical and microwave fields uses coherent superposition of the $m_s = \pm 1$ ground spin states in a NV center. As illustrated in Fig. 9, this superposition can couple to a pair of microwave fields via the transitions to the m_s=0 ground spin state and to a pair of optical fields via the electric dipole transitions to an excited state, such as the A_2 state. To demonstrate that this energy level structure can enable the interfacing between

optical and microwave fields, we first map or encode the relative phase of the two microwave fields into the relative phase of a superposition spin state (see Fig. 9a). This relative phase is then read out by the two optical fields (see Fig. 9b).

Figure 10 shows the experimental results on the transfer of phase information from microwave fields to the optical fields. In these experiments, we first encode the relative microwave phase in a spin coherence and then read out the phase information via a dark-state dependent process. A closely related approach is also used for the transfer of phase information from optical to microwave fields, for which we encode the relative optical phase into a spin coherence via optical pumping into the dark state and then retrieve the phase information with a pair of microwave fields, as discussed in detail in [7].

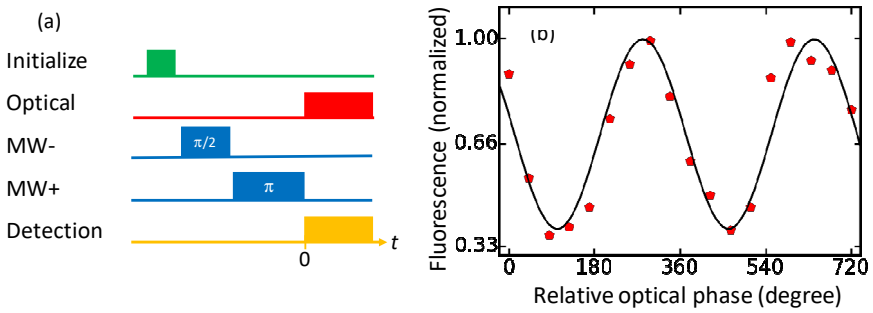

Fig. 10. a) Pulse sequence for the transfer of phase information from microwave to optical fields. A NV is initialized in the m_s=0 state. The two MW pulses prepare the NV in a superposition of m_s=±1 states. The Raman-resonant optical pulse pair then retrieves the phase information of the superposition spin state. (b) Fluorescence from state A_2 detected as a function of relative optical phase, effectively reading out the relative microwave phase and transferring the phase information from the microwave to the optical fields.

iv) Robust and nonreciprocal transport in phononic waveguides

We have been developing non-reciprocal phononic waveguide concepts that rely on dynamic modulation of nanoelectromechanical structures, which would allow transmission or blocking of phonons on-demand, and depending on propagation direction. We are employing 3 distinct approaches to achieve this result – i) the use of linear piezoelectric stiffening, i.e. changing the electrical boundary conditions of the mechanical structure modifies the phonon propagation, ii) the use of nonlinear piezoelectric coupling, i.e. forcing different acoustic waves to transfer momentum and produce a non-reciprocal modulation, and iii) employing topological pumping to produce robust transport of phonons.

a) Demonstration of a mechanical topological pump [8]

The transport of energy (e.g. in the form of phonons) through 1D waveguides can be affected by disorder, resulting in undesirable localization and backscattering. Importantly, one of the goals of this project is to produce non-reciprocal *robust* transport of phonons, i.e. guaranteeing that phonons are transported across the waveguide unidirectionally with high tolerance to disorder that might occur in space or time. For this, we can derive inspiration from the quantized disorder-resilient transport that is observable in 2D topological insulators with broken time-reversal symmetry, e.g., the edge currents of Chern insulators that are robust against damage and disorder. In this context, it has been previously shown that a topological pump can reduce this higher-dimensional topological insulator phenomena to lower dimensionality by utilizing a pumping parameter (either space or time) as an artificial dimension. We were able to demonstrate the first temporal topological pump that produces on-demand, robust transport of mechanical energy using a 1D magneto-mechanical metamaterial (see Fig. 11). The experiment was performed at extremely low frequencies (100 - 150 Hz) but may be extensible to phonon frequencies that satisfy the broader goals of this work. We also demonstrated that this pump is resilient to defects occurring in both space and time.

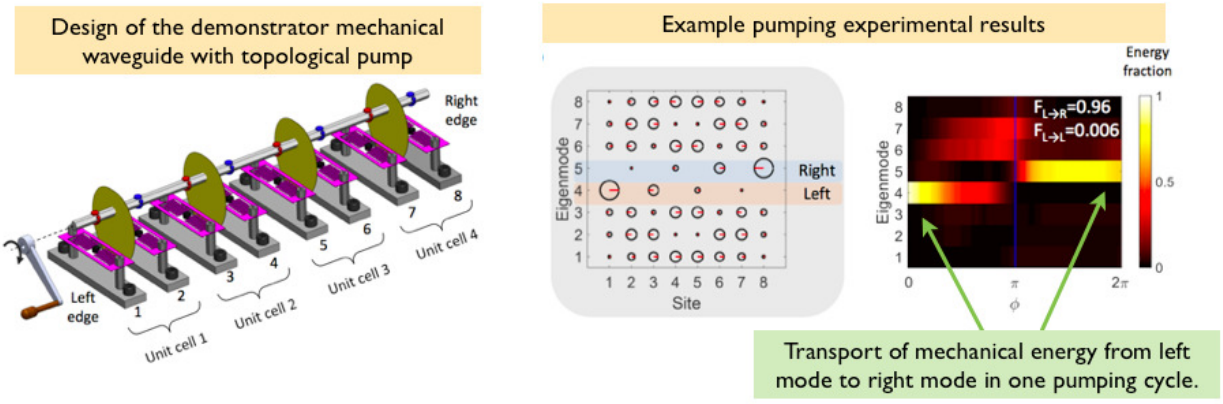

Fig 11. Schematic/design of the topological pump operating for 100-150 Hz mechanical excitations. We demonstrate pumping [8] through robust transport of energy across the 1D waveguide over one pumping cycle.

b) Continuing development of a nanoelectromechanical non-reciprocal waveguide [9]

Recently, we learned that spatio-temporal modulation of a distributed chain of resonators produces a unidirectional waveguiding channel via the Synthetic Hall Effect (see Peterson et al,

Phys. Rev. Lett. 123, 063901, 2019 and S. Kim et al APL Photonics 6, 011301, 2021). Accordingly, we have been developing a nanoelectromechanical coupled-resonator waveguide that produces this effect for phonons at high frequencies, and can permit unidirectional phonon routing.

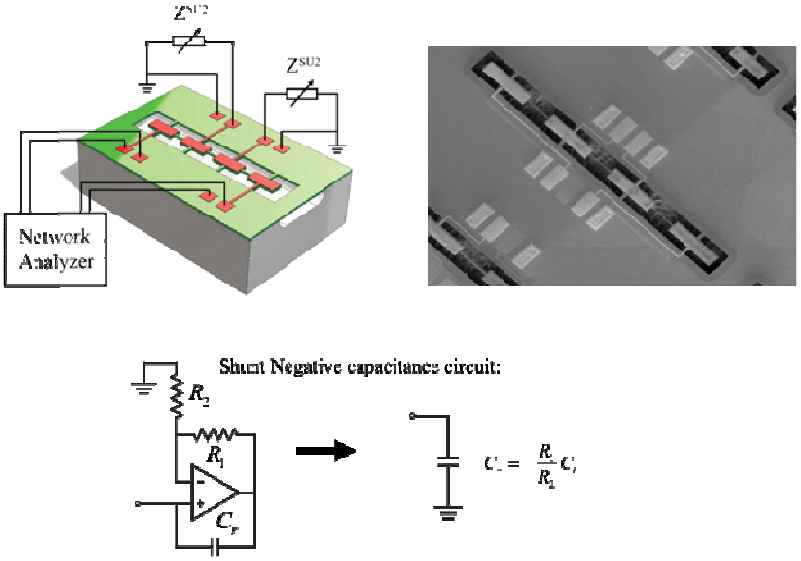

Fig 12. Schematic and SEM of a non-reciprocal phononic waveguide, still under development. We utilize a time-varying negative capacitive load on the central two resonators (ZSU1 and ZSU2) to produce a synthetic Hall effect that leads to nonreciprocity.

Our design shown in Fig. 12 is a coupled resonator array that operates for mechanical excitations around 8-16 MHz. In the future this design can be adapted to much higher frequencies in the GHz regime. The principle of operation is to spatiotemporally modulate the mechanical resonators using dynamic electromechanical loading. Specifically, we apply "negative" capacitive loads on the central two resonators as shown in Fig. 12 with locally modulated capacitance value. This changes the boundary conditions on the piezoelectric material, leading to a change in the local acoustic moduli. The result of the operation is the creation of synthetic electric and magnetic fields for phonons, which then leads to a non-reciprocal propagation channel. The device is currently still under development, but we provide here an overview of the fabrication and early measurements.

Fabrication begins with e-beam evaporation of platinum on a high resistivity Si wafer. Photolithography and lift-off was used to pattern the bottom electrode layout. Subsequently, high oriented aluminum nitride was deposited by sputtering, followed by deposition of silicon nitride

in PECVD as hard-mask for etching piezoelectric film. Photolithography is used to define etching trench on the hard-mask and AlN was anisotropically removed by ICP RIE. The hard-mask was removed by dipping in 49% HF, and a second hard-mask (SiNx, PECVD) was deposited by PECVD for wet etching of VIA. Isotropic etching was realized in AZ 400K developer at 80 degree Celsius. After removing the second hard-mask in HF, aluminum was deposited by e-beam evaporation. Photolithography and lift-off process yielded the top electrode layer. Finally, highly selective isotropic etching of Si was done using XeF_2 gas to fully release the whole structure.

We experimentally test nonreciprocal phonon propagation using an S-parameter measurement with a network analyzer (Keysight ENA E8050A). First, an impedance standard substrate is used as calibration chip to calibrate RF probe by configurations of open, short, load and thru. A GSGSG probe is used to contact the top-surface exposed aluminum pad on the device to characterize S12/S21 performance.

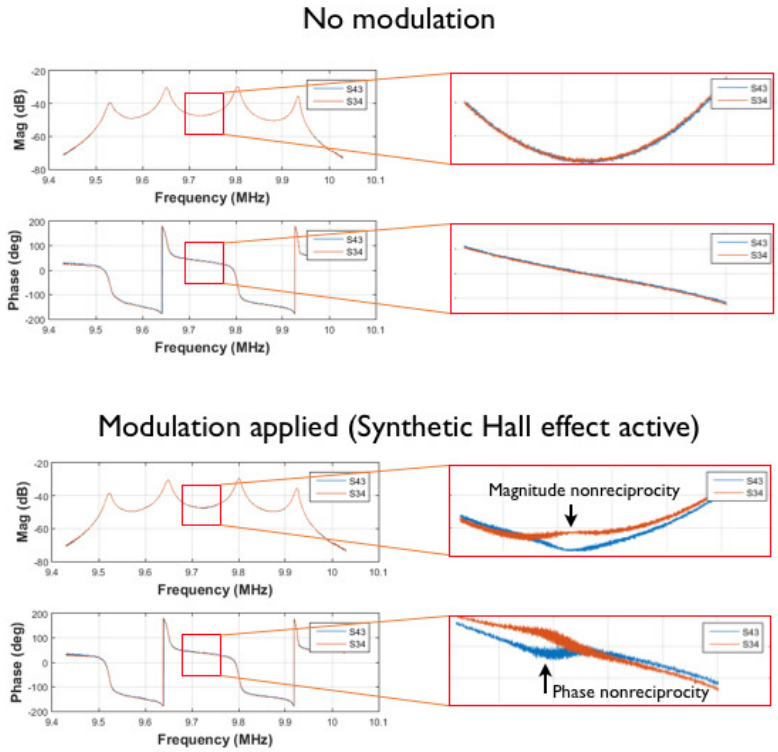

Fig 13. Preliminary measurement of the waveguiding transfer function through the system, showing the 4 poles corresponding to the 4 degrees of freedom in the waveguide. Results show that applying a spatiotemporally varying negative capacitance on the middle two resonators leads to a clearly observable nonreciprocity (see "modulation applied" case), while there is no nonreciprocity when modulation is not applied.

Unpublished results from our preliminary experiments are extremely promising and already show nonreciprocity in both amplitude and phase response (see Fig 13). While at the moment the nonreciprocity in magnitude is only about 0.6 dB, our modeling indicates that with some design modifications, and longer resonator chains, we can obtain several 10's of dB of nonreciprocity and low insertion loss. These devices are currently in production and we will be preparing a journal paper on this result soon.

3. PUBLICATIONS

[1] Ignas Lekavicius, Thein Oo, and Hailin Wang, "*Diamond Lamb wave spin-mechanical resonators with optically coherent nitrogen vacancy centers*," J. Appl. Phys. 126, 214301 (2019).

[2] Ignas Lekavicius, Thein Oo, and Hailin Wang, "*Optical coherence of implanted silicon vacancy centers in thin diamond membranes*," Optics Express 27, 31299 (2019).

[3] Mark C. Kuzyk and Hailin Wang, "*Scaling* p*hononic quantum network of solid-state spins with closed mechanical subsystems*," Phys. Rev. X 8, 041027 (2018).

[4] Xinzhu Li, Mark C. Kuzyk, and Hailin Wang, "*Honeycomb phononic network with closed mechanical subsystems*," Phys. Rev. Applied **11,** 064037 (2019).

[5] D. Andrew Golter, Thein Oo, Mayra Amezcua, Ignas Lekavicius, K.A. Stewart, and Hailin Wang, "*Coupling a surface acoustic wave to an electron spin in diamond via a dark state,*" Phys. Rev. X **6**, 041060 (2016).

[6] Hailin Wang and Ignas Lekavicius, "*Coupling spins to nanomechanical resonators: Toward quantum spin-mechanics*," Appl. Phys. Lett. 117, 230501 (2020).

[7] Ignas Lekavicius, D. Andrew Golter, Thein Oo, and Hailin Wang, "*Transfer of phase information between microwave and optical fields via an electron spin,*" Phys. Rev. Lett. **119**, 063601 (2017).

[8] I. H. Grinberg, M. Lin, C. Harris, W. A. Benalcazar, C. W. Peterson, T. L. Hughes, G. Bahl, "*Robust temporal pumping in a magneto-mechanical topological insulator*," Nature Communications **11**, 974 (2020).

[9] S. Kim, D.B. Sohn, C.W. Peterson, G. Bahl, "*On-chip optical non-reciprocity through a synthetic Hall effect for photons*," APL Photonics **6**, 011301 (2021).

4. REPORT OF INVENTIONS

[1] Hailin Wang and Mark C. Kuzyk, “Phononic quantum networks of solid-state spins with alternating and frequency-selective waveguides,” Patent application No. 16293555.

[2] A provisional patent on graded soft oxygen etching for improving surface properties of color centers in thin diamond membranes has been filed.